Chemistry Europe
European Chemical Societies Publishing
Batteries & Supercaps

RESEARCH ARTICLE OPEN ACCESS

A Mechanical Engineering Approach Toward Practical Calcium Metal Anodes with Improved Electrochemical Performance

Sibylle Riedel[1] | Laurin Kahnt[1] | Christoph Kiesl[2] | Priya Ganesan[1] | Argjend Blakaj[1] | Liping Wang[3] | Christian Bäucker[1] | Yulia Ivanisenko[4] | Maximilian Fichtner[1,4] | Zhirong Zhao-Karger[1,4]

[1]Helmholtz Institute Ulm (HIU), Electrochemical Energy Storage, Ulm, Germany | [2]fem Research Institute, Department of Electrochemical Energy Systems, Schwäbisch Gmünd, Germany | [3]Ulm University, Institute for Organic Chemistry II and Advanced Materials, Ulm, Germany | [4]Institute of Nanotechnology (INT), Karlsruhe Institute of Technology (KIT), Eggenstein-Leopoldshafen, Germany

Correspondence: Sibylle Riedel (Sibylle.Riedel@kit.edu) | Zhirong Zhao-Karger (Zhirong.Zhao-Karger@kit.edu)

Received: 22 October 2025 | **Revised:** 23 March 2026 | **Accepted:** 23 March 2026

Keywords: calcium batteries | foil | mechanical property | metal anode

ABSTRACT

Rechargeable calcium (Ca) metal batteries present an exciting opportunity for electrochemical systems offering high energy density at low costs. Although Ca possesses intrinsic advantages as a metal anode, the feasibility of fabricating thin Ca metal foils for use as practical electrodes remains unexplored. This represents a critical objective for the realization of Ca metal batteries, while it currently limits the research progress in this area. In this study, we introduce a straightforward and effective method for producing Ca foils with a thickness of approximately 100 µm from inexpensive Ca metal chunks. Additionally, we demonstrate that mechanical deformation of Ca can induce alterations in hardness, structural features, and electrochemical properties. The as-prepared Ca foils exhibit enhanced electrochemical performance underscoring that mechanical processing is a key parameter controlling the electrochemical reliability of Ca metal anodes and provides a scalable pathway toward more practical Ca metal battery architectures. This processing method could significantly contribute to the advancement of the research and development of Ca batteries.

1 | Introduction

Rechargeable metal batteries that go beyond lithium (Li) have become increasingly attractive for energy storage due to several reasons, such as the abundant availability of raw materials, potentially low production costs, and enhanced safety. Calcium (Ca) metal batteries are one promising option and have recently attracted growing research interest. The Ca metal anode stands out due to its low redox potential (−2.87 V *vs.* SHE) and high theoretical volumetric capacity (2073 mAh cm^{-3}). These values are comparable to those of Li (−3.04 V *vs.* SHE, 2062 mAh cm^{-3}) [1, 2].

At present, the commercially available Ca foils have a typical thickness of several hundred µm and are relatively expensive. However, the high price is also due to the small production and order units (e.g., 2 pcs, ∼500 µm, 25 cm^2, 896 $ ≙ 224 $ g^{-1}) [3]. For this reason, most groups in this area of research prepare the Ca metal anodes through a simple compression (squeezing) of Ca pieces/chunks or Ca granules (Ca chunks, ∼0.36 $ g^{-1}; Ca granules, ∼1.23 $ g^{-1}) [4, 5] into Ca discs [6–11]. Nevertheless, these preparation methods still suffer from poor data reproducibility. In addition, Ca anodes produced in this way are very limited in area. An advantage of using Ca granules is that the thickness of the electrode can be determined by the amount of weighed material, since the diameter is defined by the pressing tool. However, the disadvantage is that the particle boundaries (interfaces between granules) can differ greatly from electrode to electrode, which affects the reproducibility of research data. Alternatively, pressing a single Ca piece can avoid such interfacial issues, but the resulting

electrode thickness strongly depends on the initial chunk size. This makes it difficult to manufacture a bunch of electrodes of uniform thickness. Furthermore, depending on the thickness, there are difficulties to define the diameter of the electrodes, as punching out discs of required size can be challenging. To overcome these problems, we have developed a combined compression and rolling process to yield up to 100-µm thin Ca metal foils, which can be easily punched out into the desired size. The as-prepared Ca foils were characterized by diffractometry and microscopy techniques and electrochemical methods. Comparative investigations show that the obtained Ca foils exhibit significantly improved electrochemical performance and data reproducibility compared with the two commonly used types of Ca discs, which are prepared only by compression of granules or chunks. Furthermore, thinner Ca foils reduce excess Ca, which leads to higher energy density at cell level and thus represents a step toward practical application. Beyond enabling thinner Ca electrodes, we demonstrate that mechanical deformation during processing alters the microstructure and mechanical properties of Ca metal, which in turn significantly improves the electrochemical reliability and reproducibility of Ca metal electrodes. This establishes a direct processing–structure–electrochemistry relationship that is critical for the development of practical Ca metal batteries.

2 | Results and Discussion

2.1 | Fabrication of the Different Ca Electrodes

Two commercially available Ca sources, Ca metal chunks (99%, ~0.36 $ g^{-1}) [5] and Ca metal granules (99.5%, ~1.23 $ g^{-1}) [4], were used in this study. Ca chunks were initially compressed to a thickness (THK) of 600–900 µm and then gradually rolled to 100 µm with a calendering machine to obtain the Ca foils (Figure 1a). Ca granules were compressed in a mold to form a disc (THK = 700 µm) (Figure 1b). More detailed information about the procedures is given in the experimental section. In the following, the electrodes are referred to as Ca disc, Ca foil, and Ca pellet (Figure 1).

2.2 | Analysis of the Different Ca Electrodes

The three different types of electrodes were first examined using cross-section scanning electron microscopy / energy dispersive X-ray spectroscopy (SEM/EDX) (Figure 2) and focused ion beam (FIB)-SEM/EDX (Figure S1) to figure out differences on the surface and in the bulk material. As expected, the unpolished Ca samples showed oxygen contamination at the surface, but as this layer is less than 5 µm (Figure S1), it can be removed in the polishing process prior to cell assembly. A slightly thicker oxide layer observed in the samples of Figure 2 is most likely caused by the handling and transfer of the cut samples. Overall, all samples show low oxygen contamination, with the Ca foil exhibiting the lowest level and the most homogeneous Ca distribution.

To investigate further differences between the Ca samples, X-ray diffraction (XRD) in reflection (Bragg–Brentano) mode was carried out. The freshly polished samples were measured under argon (Ar) atmosphere using a PEEK dome (PEEK, polyether ether ketone). For comparison, measurements were also performed on the starting materials. Details of the sample preparation are provided in the experimental section. Relative to the reference pattern, the Ca chunk shows enhanced intensity in the [111] reflection compared to [200] in contrast to Ca granules. Comparing the [222] and [311] reflections, the [222] reflection shows increased intensity for Ca chunk with regard to the reference pattern. For Ca granules, this is not the case. However, this difference may arise from sample preparation effects, particularly in the reflection [111] as the Ca granules were embedded between two Kapton foils that contribute

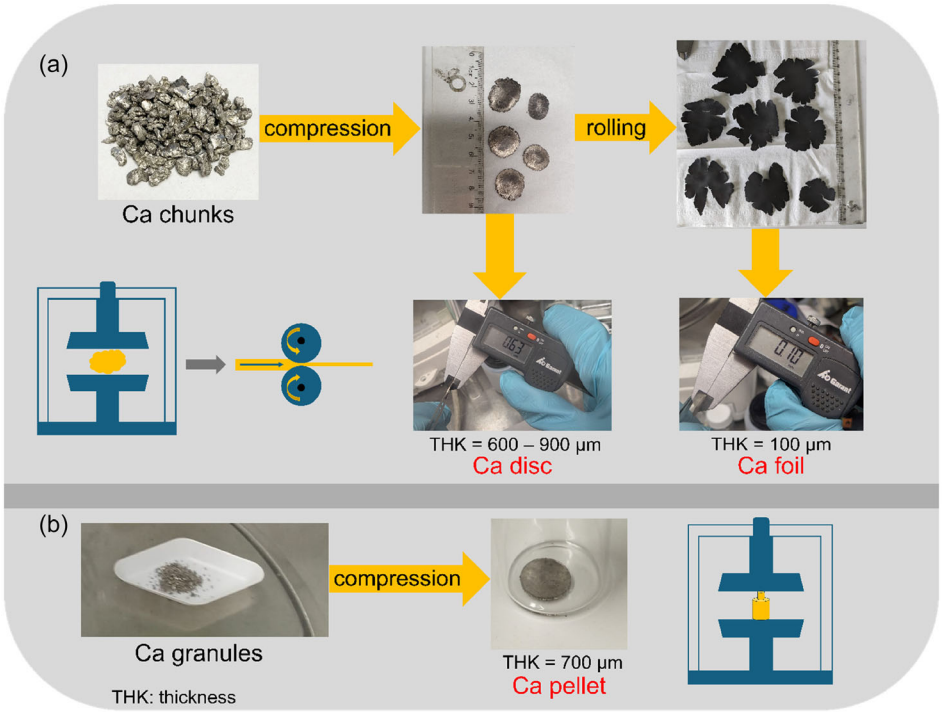

FIGURE 1 | Schematic illustration and photographs of the production process of Ca disc and Ca foil starting from Ca chunks (a) and Ca pellet starting from Ca granules (b).

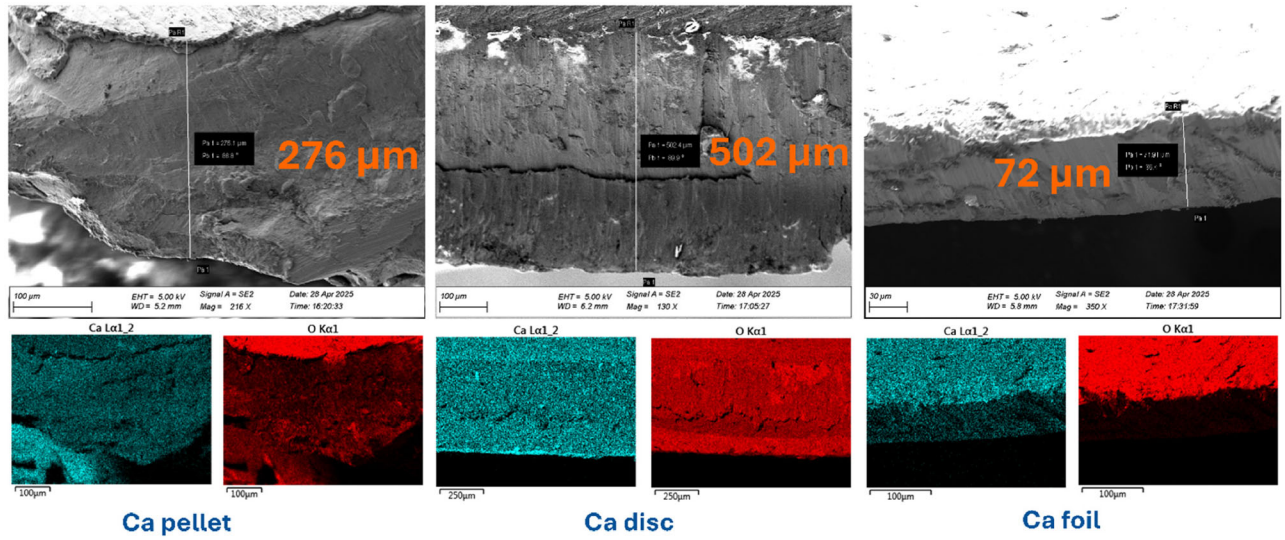

FIGURE 2 | Cross-sectional SEM/EDX of the different Ca types demonstrating the reduced thickness and oxygen contamination of Ca foil (unpolished).

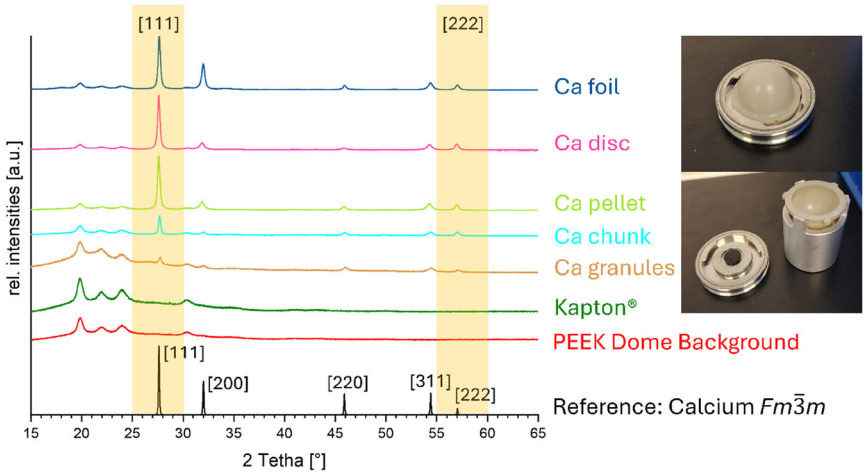

FIGURE 3 | XRD pattern of the different Ca samples (polished) and Ca sources (pristine). Insets: photographs of PEEK dome holder.

a strong background in this region. A more detailed view of the diffraction patterns of the starting materials is provided in Figure S2. The reflection positions are consistent with the reference. When now comparing the differently prepared Ca electrodes, sample-dependent variations in the reflection intensities are observed in the XRD patterns. Although the two starting materials, Ca chunk and Ca granules, differ in diffraction intensities, the resulting patterns of the Ca disc and Ca pellet exhibit very similar intensities. Relative to the reference pattern, the [111] reflection shows an increased intensity compared to the [200] reflection in the Ca disc and Ca pellet samples. Surprisingly, the reflection intensities of the Ca foil differ from those of the other Ca samples, even though the same starting material was employed for both the Ca foil and Ca disc. In addition, the pattern of the Ca foil aligns more closely with the reference pattern. This finding points toward the formation of texture with structure orientation as a result of deformation treatment (Figure 3).

As literature reports indicate that sodium (Na) impurities in Ca electrolyte salts affect electrochemical performance, it is therefore conceivable that Na impurities present in the anode material may exert a comparable effect [12]. Consequently, the Na content of the two Ca starting materials, Ca chunks and Ca granules, was determined using inductively coupled plasma optical emission spectroscopy (ICP-OES). Note that Ca disc and Ca foil used later in this work are derived from the same Ca chunk precursor. The results are as follows: 1.358×10^{-2} w% Na (relative standard deviation (%RSD), 1.198%), 7.157×10^{-3} w% Al (%RSD, 1.348%) for Ca chunks and 1.929×10^{-2} w% Na (%RSD, 2.227%), 6.929×10^{-3} w% Al (%RSD, 1.218%) for Ca granules. Aluminum was detected in both samples; its concentration is lower than that of Na but similar across materials, which likely reflects the industrial production of Ca via aluminum-based reduction of Ca oxide [13]. Na levels are low in both samples, yet about 1.4 times higher in Ca granules than in Ca chunks and should thus be considered when interpreting subsequent electrochemical data.

Importantly, by comparing Ca foil and Ca disc prepared from the same Ca chunk precursor, the effect of mechanical deformation is isolated from impurity variations. The observed electrochemical differences between these two electrodes can therefore be attributed mainly to deformation-induced structural and

morphological changes rather than to differences in elemental purity.

Subsequently, the hardness of Ca foil and Ca disc was determined (Figure S3) and Ca foil exhibited a lower hardness than Ca disc (400 *vs.* 700 N mm^{-2}). These data also indicate a change in the microstructure induced by mechanical deformation. These structural and morphological changes can also affect the electrochemical performance of Ca electrodes. This behavior is already known for some metal alloys [14].

To evaluate the electrochemical properties of different types of Ca metal electrodes, standard setups using 0.3 M $Ca[B(hfip)_4]_2$ in DME (DME, dimethoxyethane) as electrolyte were carried out [10, 15]. Detailed information can be found in the experimental section.

2.3 | Electrochemical Investigation of the Different Ca Electrodes

2.3.1 | Ca Metal as Counter Electrode

The stripping–plating cyclic voltammetry (CV) experiments show significant changes for the Ca foil in comparison to the pellet and disc samples. While Ca pellet showed the fastest activation (Figure 4e) and the highest current response, the Ca foil performed significantly better in terms of stability. The Ca disc ranged in between. The results for Ca pellet were expected due to the larger surface area of the electrode, but it also shows the lowest stability out of these three types (Figure 4f). The high stability of the Ca foil can be seen in particular in Figure 4d, as it shows perfect overlap for at least 30 cycles. Furthermore, Ca pellet showed the best Coulombic efficiency (CE) in the beginning (~80%), but dropped with every subsequent cycle, whereas Ca disc and Ca foil stabilized at ~75% (Figure S4a). To further investigate the electrochemical stability of the Ca foil, galvanostatic stripping–plating experiments were conducted.

In this measurement, Ca foil again demonstrated stable performance in contrast to Ca disc and Ca pellet (Figure 5a,b, S5a–c). When Ca foil was employed as the counter electrode, stable cycling with consistently stable CE was observed following a short activation period. Notably, the CE obtained via this cycling protocol is lower than that derived from CV measurements (~50% *vs.* ~75%) (Figure S4b). Differences in CE obtained from CV and galvanostatic stripping/plating experiments are frequently observed in Ca metal systems, and similar qualitative discrepancies between CV characteristics and cycling efficiencies have been reported in previous studies on Ca metal electrodes [16, 17].

Now that stable cycling has been achieved using Ca foil as the counter electrode, Ca deposition on ccAl became possible. The corresponding electrochemical data are shown in Figure S6. As seen in the inset of Figure 5c, a gold-colored film formed on the ccAl, which energy-dispersive X-ray (EDX) analysis confirms, consists predominantly of Ca (Figure 5c). Fluoride contamination arises from electrolyte decomposition, while oxygen contamination is attributed to sample preparation, as freshly deposited Ca is highly reactive.

Notably, detectable deposition on ccAl was only achieved with Ca foil as counter electrode; Ca disc or Ca pellet did not yield observable deposits. We cannot, however, rule out that deposition occurs with a different morphology and is removed during sample preparation (*e.g.*, repeated washing with DME) or that side reactions are more prevalent with other counter electrodes, preventing detectable Ca formation. Importantly, deposition on ccAl was consistently observed when Ca foil was used as the counter electrode.

Furthermore, Ca foil reliably gave reproducible results, emphasizing its reliability as a counter electrode. To substantiate this, data from different cells with Ca foil and Ca disc as counter electrodes are shown in Figure S7a,b.

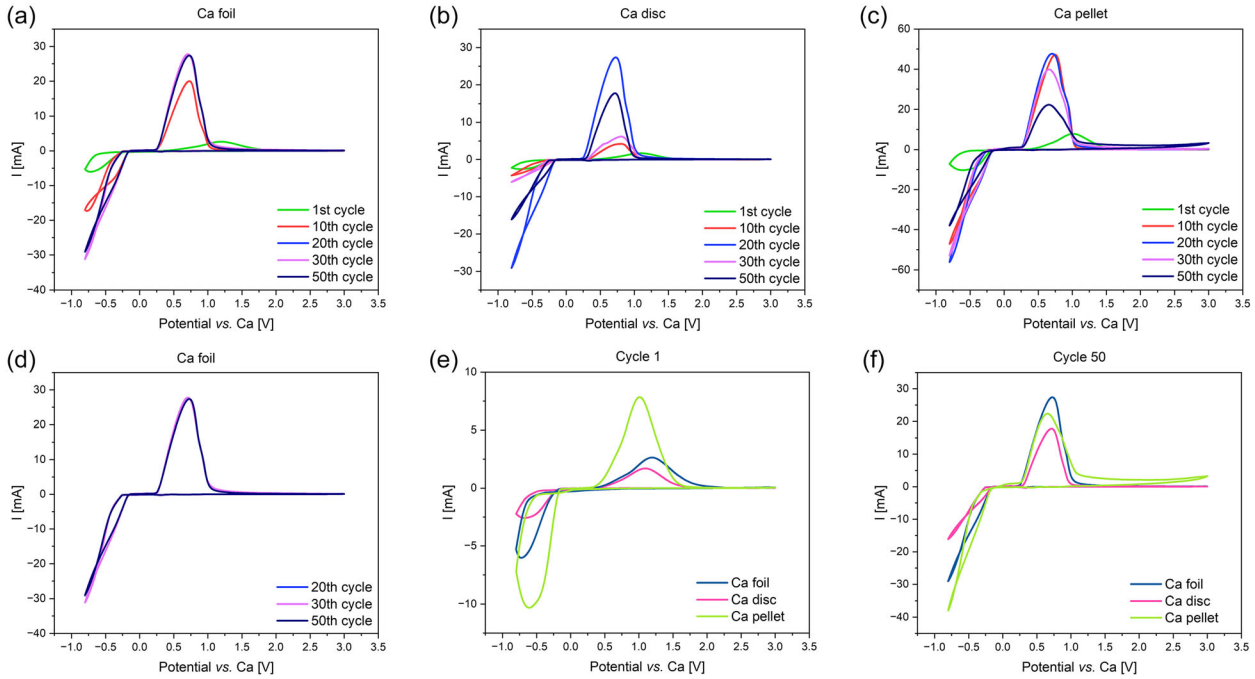

FIGURE 4 | CV 80 mV s^{-1}, −0.8–3.0 V: Ca (12 mm), $Ca[B(hfip)_4]_2$·4DME in DME, ccAl (11.8 mm) (ccAl, carbon-coated aluminum foil); (a) Ca foil, (b) Ca disc, (c) Ca pellet as counter electrode; (d) overlapping cycles of Ca foil; comparison of cycle 1 (e) and cycle 50 (f).

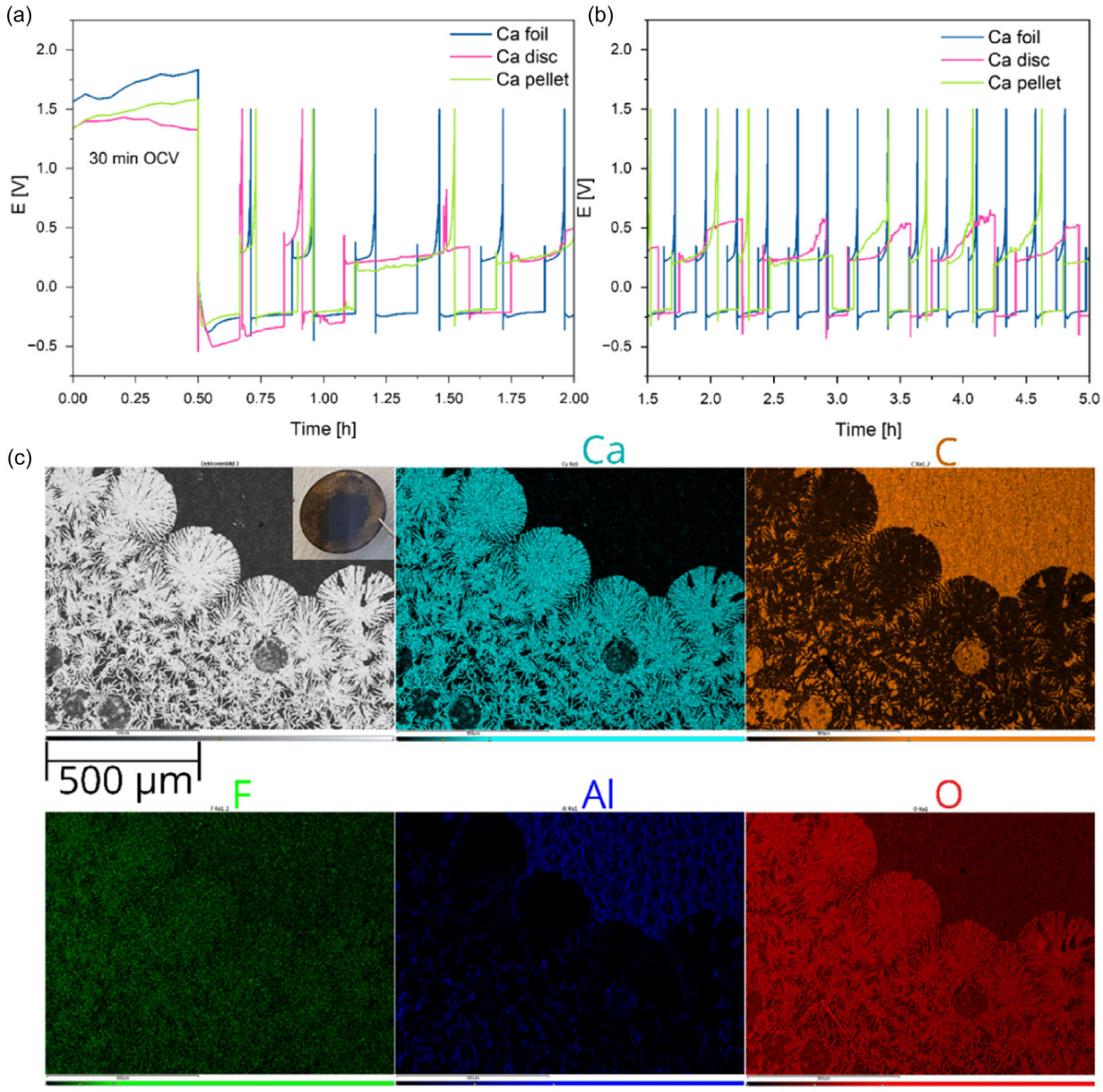

FIGURE 5 | (a,) Open circuit voltage (OCV) 30 min; galvanostatic stripping–plating 0.1 mA cm^{-2} 10 min discharge, cut/off 1.5 V or 30 min: Ca (12 mm), $Ca[B(hfip)_4]_2 \cdot 4DME$ in DME, ccAl (11.8 mm); (c) *ex situ* analysis: SEM/EDX of deposits on ccAl after—current density, 0.1 mA cm^{-2}, 10 min discharge, cut/off 1.5 V or 30 min, 10 cycles then 1 cycle 30 min discharge. Inset: photograph of deposits on ccAl.

2.3.2 | Ca Metal as Anode

Symmetrical cells were assembled to evaluate the differently manufactured Ca electrodes as anodes. Although clear electrochemical trends are observed, none of the configurations achieves ideal performance (Figure 6a,c,d). When focusing on the initial cycles, the Ca foil anode exhibits the most representative and reproducible behavior (Figures 6c, S7c).

Impedance spectroscopy (PEIS) further confirms that Ca foil shows the lowest impedance (Figure 6b) and yields the most consistent results, particularly in the first few cycles (Figure S7c,d). While the differences are less pronounced than in asymmetric cells, especially when comparing Ca foil and Ca disc (Figure S7), the reproducible short-term behavior is crucial for systematic electrolyte optimization.

Since all cells show features typically associated with soft short circuits and/or self-healing processes after prolonged operation, Ca foil was selected for further study as an anode [18, 19]. Two symmetric cells with Ca foil were subjected to galvanostatic cycling, and PEIS was recorded after 5, 20, 50, and 100 cycles (Figures S8,S9). Figure S10 compares these cells with the example in Figure 6, all of which show similar behavior in the initial cycles. Although both cells started similarly, differences in polarization and long-term stability emerge over time. PEIS data (Figures S8f,S9f) remain largely consistent, with only one notable outlier per cell: after 50 cycles for cell 1 (Figures S8d,f), in line with increased polarization, and after 20 cycles for cell 2 (Figures S9c,f), accompanied by increased polarization and spiking behavior.

Taken together, the reproducible electrochemical behavior of Ca foil as an anode supports its suitability for further development of

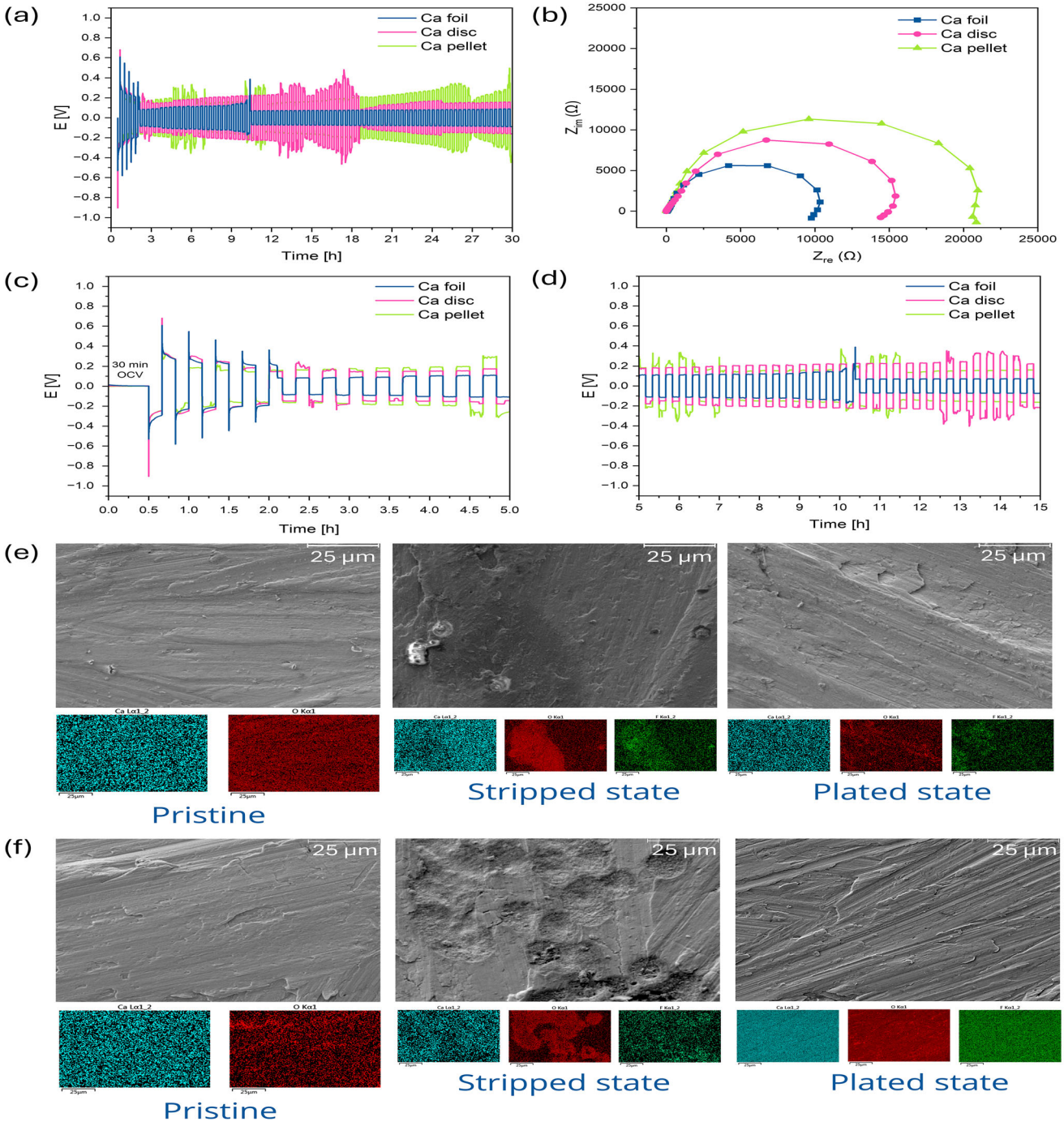

FIGURE 6 | (a–d) Symmetrical cells: Ca (12 mm), $Ca[B(hfip)_4]_2.4DME$ in DME, Ca (12 mm), (a) cycling: current density, 0.1 mA cm^{-2}, 10 min; (b) potentiostatic electrochemical impedance spectroscopy (PEIS) after 30 min resting; (c,d) zoom in at different times; (e,f) *ex situ* analysis of Ca electrodes, symmetrical cells—SEM/EDX: current density, 0.1 mA cm^{-2}, 10 min discharge / charge, 10 cycles then 1 cycle 30 min discharge; (e) Ca disc, (f) Ca foil.

Ca-based battery systems. Unlike Ca disc or Ca pellet, Ca foil maintains a nearly uniform thickness, minimizing pressure fluctuations and promoting a more homogeneous pressure distribution within the cell stack, which in turn reduces local contact variations and improves electrochemical performance.

In order to better understand the different electrochemical behavior, ex situ measurements (SEM-EDX) were performed on Ca foil and Ca disc. The corresponding electrochemical data can be seen in Figure S11. Interestingly, the Ca disc exhibits relatively smooth surfaces in both the stripped and plated states (Figure 6e). In contrast, Ca foil shows small holes in the stripped state and a smooth surface again in the plated state (Figure 6f). The elevated oxygen signals within these holes could be attributed to the high reactivity of fresh Ca surfaces. These observations in turn point to the altered microstructure of the Ca foil, which appears to lead to preferred sides for stripping. When repeating the experiments, such holes could only be found when using Ca foil.

The most obvious difference in the corresponding electrochemical data (Figure S11) is the polarization, which was significantly

higher for the Ca disc, indicating that stripping and plating are more facile on Ca foil. Furthermore, the data for Ca foil are more reproducible, whereas Ca disc frequently failed to yield comparable behavior (Figure S7), and often could not sustain 10 stable cycles (Figure S11a shows one of the few exceptions). While optimization is still required, the reproducibility of Ca foil greatly facilitates systematic studies and further improvements.

2.3.3 | Three-Electrode Measurements

To gain further insight into the system, three-electrode measurements were conducted to compare the behavior of the different Ca electrodes. In these experiments, Ca foil served as the quasi-reference electrode (RE), ccAl as the working electrode (WE), and either Ca foil or Ca disc as the counter electrode (CE). Detailed information about the cell assembly will be given in the experimental section. The data obtained for the Ca foil are shown in Figure 7g,h, and those for the Ca disc are presented in Figure S12a,b. Moreover, both cells exhibit noticeable potential differences between CE and RE, which we attribute to the cell setup and the significant size difference between the electrodes ($ø = 11$ mm *vs.* $ø = 3$ mm). Nevertheless, the use of Ca foil as counter electrode leads to substantially smaller polarization differences than Ca disc as counter electrode, in agreement with the overall dataset and further supporting the conclusion that electrochemical processes are less hindered with Ca foil. Following adequate activation (Figure S13) in the modified cell configuration, both systems display behavior comparable to that of the two-electrode setup, although markedly longer activation times are required for the Ca disc. Furthermore, the voltage dip at the onset of discharge is less pronounced when the potential is evaluated as WE *vs.* RE, indicating that this effect mainly originates from the CE. In addition, stable cycling proved more difficult to achieve when using a Ca disc as the counter electrode. In this configuration, the large thickness of the Ca disc appears to exert a more detrimental effect. Taken together, these results highlight Ca foil as a suitable and reliable material for use as both the counter electrode and the quasi-RE in the present setup.

2.3.4 | Different Ca Metal Anodes in Full Cells

With Ca disc and Ca foil as anode, we assembled full cells with 1,4-polyanthraquinone (14PAQ) as cathode material to figure out if different behavior can be observed as well [20–22]. Looking at Figure 8a,b, the performance seemed to be quite similar as both cells were showing same behavior in the 10th cycle. This comparable behavior is attributed to a failure mode that we term "incipient calcium death," for which mitigation strategies are currently being investigated. However, closer examination at cycle 2 (Figure 8c) discloses clear differences. Using Ca foil as anode resulted in higher values, discharge capacity, and voltage wise (~162 *vs.* ~194 mAh g^{-1}, ~1.82 *vs.* ~1.90 V). These results demonstrate that Ca foil also enables improved performance in full-cell configurations.

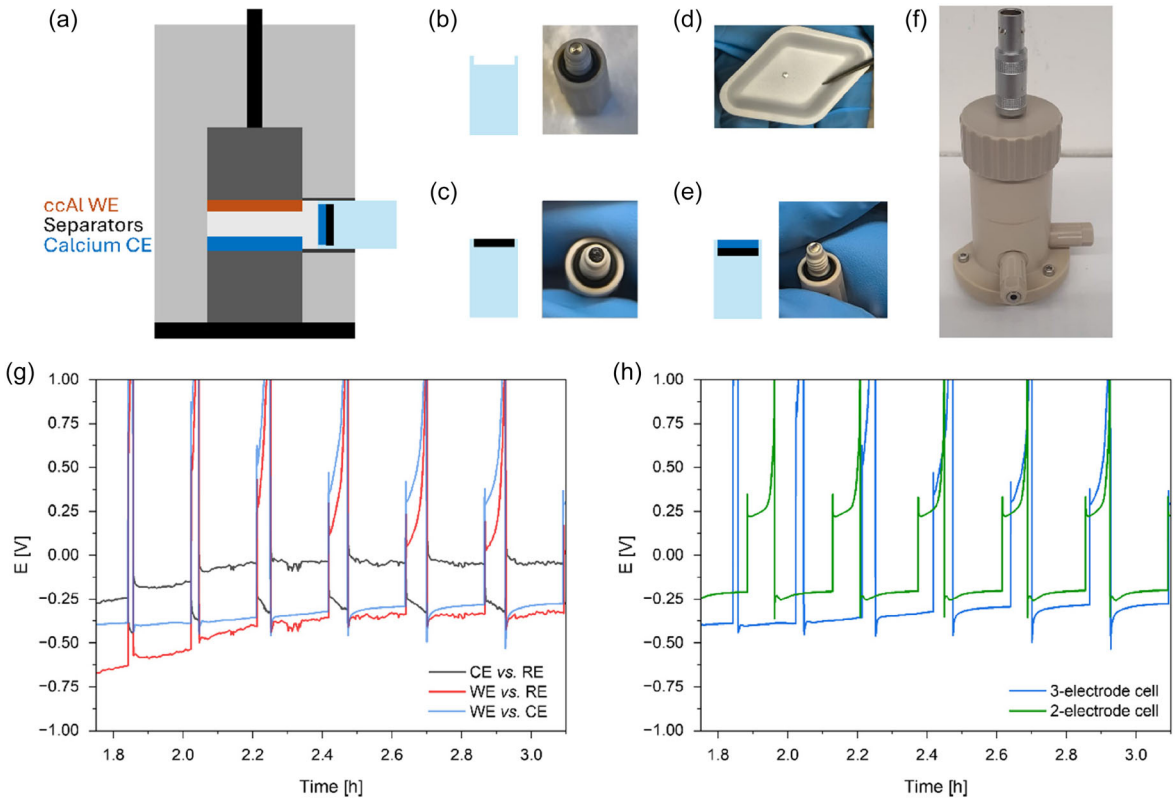

FIGURE 7 | (a) Schematic illustration of the three-electrode setup from rhd instruments; (b) reference connector; (c) reference connector with conductive carbon tape; (d) Ca foil (2 mm) as quasi-reference; (e) reference connector including Ca reference; (f) photograph of the three-electrode cell from rhd instruments; (g) galvanostatic stripping–plating 0.1 mA cm^{-2} 10 min discharge, cut/off 1.5 V or 30 min: Ca foil (11 mm), $Ca[B(hfip)_4]_2 \cdot 4DME$ in DME, ccAl (11 mm); Ca foil (3 mm) as quasi-reference; (h) comparison of three- and two-electrode cell.

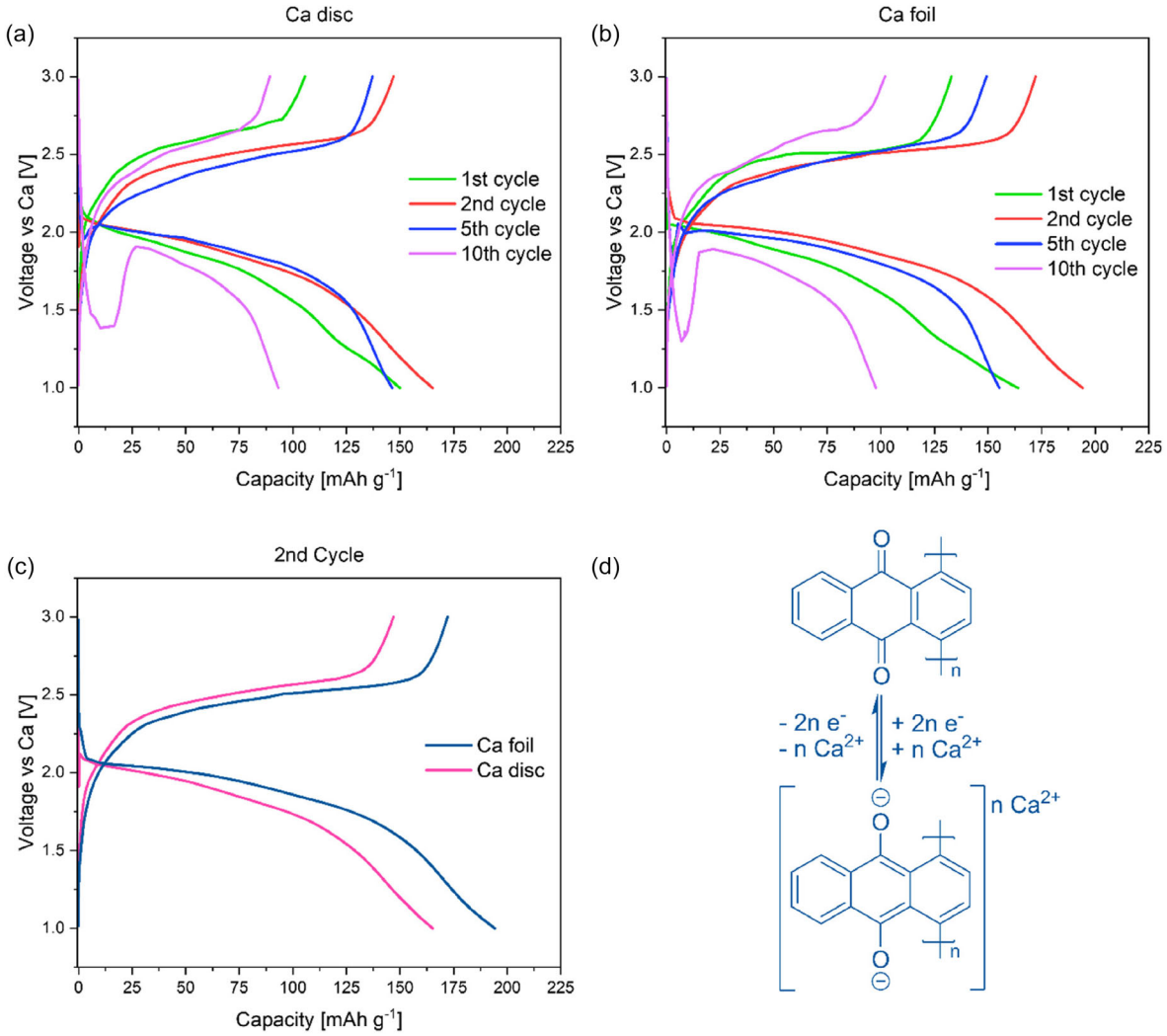

FIGURE 8 | (a–c) Galvanostatic cycling of Ca, 14PAQ cells: Ca (13 mm), $Ca[B(hfip)_4]_2{\cdot}4DME$ in DME, 14PAQ (12 mm); current density, 130 mA g^{-1}; (a) Ca disc, (b) Ca foil as anode; (c) comparison of the second cycle of Ca foil and Ca disc; (d) structure and redox process of 14PAQ (1C = 260 mAh g^{-1}).

3 | Conclusion

We successfully fabricated thin Ca foil with a thickness of 100 µm, which simplifies the handling in the lab and shows enhanced electrochemical performance. Cells using Ca foils as counter electrodes or as anodes and $Ca[B(hfip)_4]_2$ in DME as electrolyte showed higher stability, improved performance, and enhanced reproducibility compared to conventional Ca electrodes, especially in asymmetrical cells. Furthermore, the manufacturing method of the Ca electrode appears to be more critical than minor variations in the purity and composition of the starting materials. In addition, this processing method is scalable to larger sheets of foils, suitable for pouch cell assembly. An initial scaling test for the preparation of foils with larger area has already been carried out. A photograph of such a foil (~100 cm^2) prepared from a Ca ingot can be seen in Figure S14. The performance of electrodes out of this larger sheet is currently being investigated. The foils currently being prepared have a maximum surface area of ~20 cm^2 and exhibit the reliable and reproducible behavior described above. Beyond the fabrication of thin Ca foils, this work demonstrates that mechanical processing plays a decisive role in defining the electrochemical behavior of Ca metal electrodes. The deformation-induced microstructural homogenization results in improved electrochemical reliability and reproducibility, which are essential prerequisites for the systematic development of practical Ca metal battery systems. With reliable foils in hand, it is easier to work on optimizing cell life using various approaches, such as different electrolyte compositions for forming a stable SEI (solid electrolyte interphase) or investigating various artificial SEI's. This approach enables more practical and reproducible Ca electrodes, thus advancing the development for rechargeable Ca metal batteries.

4 | Experimental Section

4.1 | Chemicals, Materials, and Preparations

Unless otherwise stated, the following starting materials were used as purchased: Ca chunks (99%, Thermo Fisher Scientific), Ca metal granules (99.5%, 16 mesh, Thermo Fisher Scientific), $Ca(BH_4)_2{\cdot}2THF$ (Merck), DME (99.5%, extra dry, stabilized, Thermo Fisher Scientific), hexafluoroisopropanol (Hhfip, 99%, abcr), dimethylformamide (DMF, 99.8%, extra dry, Thermo Fisher Scientific), bis(cyclooctadiene)nickel(0) ($Ni(COD)_2$, 98%, abcr), 1,4-dichloroanthraquinone (>98%, TCI), 2,2′-bipyridyl (BPY, >99%, TCI), 1,5-cyclooctadiene (COD, 99+%, stabilized,

Thermo Fisher Scientific), hydrochloric acid (32%, Supelco, Merck), methanol (>99.9%, Sigma–Aldrich), disodium ethylenediaminetetraacetate (Na_2EDTA, Supelco, Merck), chloroform (99+%, extra pure, stabilized, Thermo Fisher Scientific). Ketjenblack EC-600JD was used as conductive carbon, Na alginate as binder (Sigma–Aldrich), ccAl (En Safe 20, Armor Battery Films), Whatman glass fiber separator (GF/C), Celgard 2325 Trilayer Microporous Membrane (CG), 2032 coin cell parts (SEIKA SANGYO GMBH). DME, DMF, and Hhfip were stored over activated molecular sieves (3 Å) minimum 1 day prior to use. For asymmetric cells, ccAl was punched out into circular plates ($\varnothing$ = 11.8 mm or 11 mm) and dried at 80°C in vacuum. The prepared separators have a diameter of 16 mm or 12 mm and were dried at 230°C (GF/C) or 30°C (CG) in vacuum.

4.2 | Cathode Material

Synthesis of 14PAQ: Under Ar atmosphere, 1,4-dichloroanthraquinone (3.49 g, 12.6 mmol, 1.0 eq.) was dissolved in dry DMF (210 mL) (solution A) and $Ni(COD)_2$ (4.51 g, 16.4 mmol, 1.3 eq.), COD (1.55 mL, 1.36 g, 12.6 mmol, 1.0 eq.), and BPY (2.56 g, 16.4 mmol, 1.3 eq.) were dissolved in dry DMF (210 mL) (solution B). Under vigorous stirring, solution A was added to solution B and the reaction mixture was heated to 60 °C and maintained at this temperature for 48 h. The color of the reaction mixture changed from deep blue to black. After cooling down to room temperature, hydrochloric acid (0.5 M, 420 mL) was added, causing a brownish-yellow solid to precipitate. The solid matter was filtered out and washed with hydrochloric acid (0.5 M, 400 mL), methanol (200 mL), warm half-saturated Na_2EDTA (60 °C, 600 mL), warm water (60 °C, 200 mL), and again with methanol (200 mL) yielding a yellow powdery solid. The powder was dissolved in refluxing chloroform (66 mL) and reprecipitated with methanol (50 mL). After filtration, a bright yellow powder was observed, which was suspended in DME (80 mL) and stirred for 72 h at room temperature and then filtered off and dried for 48 h at 60 °C in vacuum. 1,4PAQ ($M_{\text{repeating unit}} = 206.20\ \text{g mol}^{-1}$, 2.58 g, 12.5 mmol, 99%) was obtained as bright yellow powdery solid. The analytical data are in agreement with those reported in literature [23].

Preparation of 14PAQ-Cathode: 14PAQ (400 mg) was dissolved in chloroform (50 mL), mortared Ketjenblack (200 mg) was added, and the mixture was stirred for 2 h at room temperature. After that, the solvent was removed under reduced pressure (40 °C). The resulting black powder was ball milled (powder to ball (Si_3N_4); 1:25; 200 rpm 10 min, 5 min rest, 50 cycles) to obtain the 14PAQ-composite.

Slurry Preparation: 90 mg of 14PAQ-composite, 10 mg of Na alginate (2.5 w% in H_2O), 100 µL H_2O, and 50 µL iso-propanol were mixed and cast onto ccAl, predried at room temperature, and then dried in vacuum at 60 °C overnight. After that, circular plates were punched out ($\varnothing$ = 12 mm). The cathodes contain 60% of active material and an average loading of 1.5 mg cm^{-2}.

4.3 | Electrolyte

$Ca[B(hfip)_4]_2$·4DME synthesis and preparation: Under Ar atmosphere, $Ca(BH_4)_2$·2THF (10.0 g, 46.8 mmol, 1 eq.) is suspended in DME (200 mL). Hhfip (44.0 mL, 416 mmol, 8.9 eq.) is then added dropwise (gas evolution) to give a clear solution. The solution is then left to stir overnight at room temperature (rt). The next day, the solvent is removed under reduced pressure ($\sim 10^{-2}$ mbar, rt to 60 °C). In an Ar-filled glovebox, the resulting white powder is transferred to a BÜCHI tube and dried for 24 h in a BÜCHI oven ($\sim 10^{-2}$ mbar, 60 °C, 5 rpm). The product $Ca[B(hfip)_4]_2$·4DME (76.1 g, 43.2 mmol, 92%) is obtained as a white crystalline powder. The analytical data are in agreement with those reported in literature [10, 15]. The white crystalline powder was dissolved in dry DME to get a 0.3 M solution.

4.4 | Anode Materials

Unless otherwise stated, the processes were carried out under ambident conditions (air, rt). **Ca pellet**: Ca metal granules (120 mg) were put in a mold ($\varnothing$ = 12 mm) and pressed (12 t) to circular plates (THK = 700 µm) (Manual Hydraulic Press, Specac). **Ca disc**: Ca chunks were pressed into sheets (THK = 600–900 µm) and punched out into circular plates ($\varnothing$ = 11 mm, 12 mm, or 13 mm) (Manual Hydraulic Press, Specac). **Ca foil**: The Ca sheets (THK = 600–900 µm) were gradually rolled down at room temperature to 100-µm foils using a calendering machine (speed 10 mm s^{-1}, stepwise 100 µm steps in the beginning (until 250-µm thickness), later 30 µm steps; 9.18 → 19.25 kbar (details in supporting information, Table S1–S4), electric hot rolling press with variable speed, MSK-HRP-01, MTI Corporation). The Ca foils were also punched into circular plates ($\varnothing$ = 11 mm, 12 mm, or 13 mm). The prepared Ca electrodes were transferred immediately to an Ar-filled glovebox. Before battery assembling, both sides were polished using a polishing tool with a diamond head [24] to a mirror like surface.

4.5 | Battery Assembling

The coin cells were assembled in an Ar-filled glovebox. A sandwich separator setup (CG / GF/C / CG) and 90 µL of electrolyte solution were used for all cells except the CV cells (2 GF/C, 80 µL). To adjust the pressure in the cells, spacers with different thickness were added. An overview of this can be seen in Table S5. The three-electrode cell was also assembled in an Ar-filled glovebox. The sandwich separator setup and 90 µL of electrolyte were likewise used. The Ca foil ($\varnothing$ = 2 mm) serving as the quasi-RE was attached to the reference connector using two layers of conductive carbon tape (THK = 125 µm, Science Services) (Figure 7b–e). For the RE, two GF/C separators ($\varnothing$ = 3 mm) were inserted to ensure proper separation and contact. All cells were rested for 30 min except the full cells (1 h).

4.6 | Analytical Data—SEM/EDX, FIB/SEM/EDX

All the sample preparation was carried out in Ar-filled glove box. The surface morphology and chemical composition of the Ca surfaces were analyzed using different devices. One is a scanning electron microscope (SEM, Gemini SEM 300, Carl Zeiss Microscopy) equipped with EDX. Measurements were performed at 8 kV with the secondary electron (SE) detector. Focused ion beam (FIB) investigations were conducted in a separate SEM (Auriga 60, Carl Zeiss Microscopy) also equipped with EDX. These measurements were carried out at 2.0 kV using the InLens detector. Prior

to milling, a protective Pt bar was deposited on the Ca surface to minimize curtaining artifacts. To prevent reactions with oxygen and/or moisture, a sealed transfer module (Kammrath & Weiss, Schwerte) was employed to safely transport the specimens between the glovebox and the SEM (data regarding Figures 5, S1). Another device used is a Zeiss crossbeam 340 microscope. The pristine and cycled electrodes were placed on the carbon tape and transferred to the microscope in an airtight container. The measurements were performed at an accelerating voltage of 5 kV and the SE were detected with Everhart–Thornley detector (data regarding Figures 2, 7). FIB/SEM/EDX: Pristine samples without polishing. SEM/EDX: For cross-section, the unpolished pristine samples were cut inside an Ar-filled glovebox prior to the measurement. The pristine samples for comparison with the cycled samples were polished using a polishing tool with a diamond head [24] before measurement. The cycled samples were washed with dry DME (3×) and dried before. All preparation steps were done in an Ar-filled glovebox.

4.7 | Analytical Data—Surface X-Ray Diffraction (SXRD)

The crystal structure of the Ca samples was examined using surface X-ray diffraction (SXRD) on an Empyrean diffractometer (Malvern Panalytical, Netherlands) with Cu Kα radiation (λ = 0.15418 nm) operated at 45 kV and 40 mA, with a step size of 0.0167°. To prevent oxidation, samples were freshly polished and loaded into a PEEK dome inside an Ar-filled glovebox and measured without air exposure. A borosilicate glass disc was used to record the background pattern originating solely from the PEEK dome. Both starting materials were measured using the same procedure as the fabricated electrodes. For the Ca granules, the powder was embedded between two Kapton foils and mounted in the sample holder in the same manner as the other samples. For the Ca chunks, a piece with a flat side was selected and carefully aligned in the holder. The background contribution of the Kapton foil was determined by measuring it separately under the same PEEK dome. Figure S15 presents a schematic illustration of the measurement setup.

4.8 | Analytical Data—ICP-OES

For ICP-OES analysis, 124.40 mg (Ca granules) and 125.19 mg (Ca chunks) were dissolved/reacted with nitric acid (1 M) and then diluted to 100 mL using a volumetric flask. Measurements were performed using a SPECTRO ARCOS (ARCOS FHS12) ICP-OES from Spectro Analytical Instruments GmbH, and Na was determined by the standard addition method.

4.9 | Analytical Data—Instrumented Indentation Testing

Hardness measurements were performed using a Fischer HM500 nanoindenter equipped with a Vickers diamond indenter, in accordance with DIN EN ISO 14577. The maximum applied load was 5 mN, with a loading time of 10 s and a holding time under a maximum load of 10 s before unloading. The waiting time with retracted indenter tip prior to measurement was 120 s, ensuring thermal and mechanical stabilization of the system. The instrument continuously recorded the force–displacement curve, from which characteristic mechanical parameters were derived. Data were processed following the Oliver–Pharr method as implemented in the device software.

4.10 | Electrochemical Data

Most of the data are collected from two-electrode cells (2032 coin cell). Symmetrical and asymmetrical cells were employed to evaluate the different types of Ca electrodes. Ca was repeatedly plated or stripped at a current density of 0.1 mA cm^{-2} throughout the electrochemical process. CV measurements were carried out at a scan rate of 80 mV s^{-1} in a voltage range of −0.8–3.0 V *vs.* Ca/Ca^{2+}. Electrochemical impedance spectroscopy (EIS) was carried out from 1 to 100 mHz with a DC voltage amplitude of 10 mV. Three-electrode measurements were conducted using the TSC battery cell (Figure 7f) supplied by rhd instruments GmbH & Co. KG. For all these measurements, a Biologic VMP-3 potentiostat was used. Galvanostatic charge/discharge experiments were performed for the Ca–14PAQ coin cells, in a voltage range of 1.0–3.0 V *vs.* Ca/Ca^{2+} and at a C-rate of 0.5C (14PAQ: 1C = 260 mA g^{-1}) using a Biologic BCS 805 testing unit.

Acknowledgments

We would like to thank Rita Bretzler and Britta Schöne (fem Research Institute) for her support with the FIB/SEM/EDX measurements and Florian Kößler (wbk Institute of Production Science, Karlsruhe Institute of Technology) for the informative and engaging discussion of the calendering process. We would like to sincerely thank Dr. Marcel Drüschler and Dr. Christoffer Folkers-Karlsson (rhd instruments GmbH & Co. KG) for their expert guidance on the TSC battery and for the helpful and insightful discussions. Furthermore, we would like to thank the students Devran Cay and Fabian Frysztacki (Karlsruhe Institute of Technology) for their continuous support in providing the basic materials. This work was funded by the Federal Ministry of Education and Research (Bundesministerium für Bildung und Forschung, BMBF) of Germany within the project "CaSino" (03XP0487F) and the German Research Foundation (Deutsche Forschungsgemeinschaft, DFG) under project ID 390874152 (POLiS Cluster of Excellence). This work contributes to the research performed at CELEST (Center for Electrochemical Energy Storage Ulm-Karlsruhe).

Open Access funding enabled and organized by Projekt DEAL.

Conflicts of Interest

The authors declare no conflicts of interest.

Data Availability Statement

The data that support the findings of this study are openly available at Zenodo DOI: https://doi.org/10.5281/zenodo.17176985.

References

1. I. D. Hosein, "The Promise of Calcium Batteries: Open Perspectives and Fair Comparisons," *ACS Energy Letters* 6 (2021): 1560–1565.

2. Z. Li, S. Cui, J. Häcker, *et al.*, "Calcium Chemistry as A New Member of Post-Lithium Battery Family: What Can We Learn from Sodium and Magnesium Systems," *Angew. Chem. Int. Ed* 64 (2025), https://doi.org/10.1002/anie.202415942.

3. *"yourfoilscom," can be found under* http://www.yourfoils.com/html_products/calcium-foil-40.html (accessed 26 August 2025), (2025).

4. "thermofisher.com Ca Granules," can be found under https://www.thermofisher.com/order/catalog/product/042917.18?SID=srch-srp-042917.18(accessed 26 August 2025), 2025.

5. "thermofisher.com Ca Chunks," can be found under https://www.thermofisher.com/order/catalog/product/201185000?SID=srch-hj-201185000(accessed 26 August 2025), 2025.

6. S. Wu, Z. Jiang, C. Wu, *et al.*, "High-Content Carbon Layer Confined Small- Molecule/Covalent Sulfur Cathode Enables Long-Life Calcium–Sulfur Batteries in Hybrid-Ion Electrolyte," *Advanced Functional Materials* 34 (2024), https://doi.org/10.1002/adfm.202313441.

7. X. Yu, M. J. Boyer, G. S. Hwang, and A. Manthiram, "Toward a Reversible Calcium-Sulfur Battery with a Lithium-Ion Mediation Approach," *Advanced Energy Materials* 9 (2019), https://doi.org/10.1002/aenm.201803794.

8. K. Kisu, R. Mohtadi, and S. Orimo, "Calcium Metal Batteries with Long Cycle Life Using a Hydride-Based Electrolyte and Copper Sulfide Electrode," *Advancement of Science* 10 (2023), https://doi.org/10.1002/advs.202301178.

9. T. Pavčnik, J. D. Forero-Saboya, A. Ponrouch, A. Robba, R. Dominko, and J. Bitenc, "A Novel Calcium Fluorinated Alkoxyaluminate Salt as a Next Step towards Ca Metal Anode Rechargeable Batteries," *Journal of Materials Chemistry. A* 11 (2023): 14738–14747.

10. Z. Li, O. Fuhr, M. Fichtner, and Z. Zhao-Karger, "Towards Stable and Efficient Electrolytes for Room-Temperature Rechargeable Calcium Batteries," *Energy & Environmental Science* 12 (2019): 3496–3501.

11. Z. Meng, A. Reupert, Y. Tang, *et al.*, "Long-Cycle- Life Calcium Battery with a High-Capacity Conversion Cathode Enabled by a Ca^{2+}/Li^{+} Hybrid Electrolyte," *ACS Applied Materials & Interfaces* 14 (2022): 54616–54622.

12. S. A. McClary, D. M. Long, A. Sanz-Matias, *et al.*, "A Heterogeneous Oxide Enables Reversible Calcium Electrodeposition for a Calcium Battery," *ACS Energy Letters* 7 (2022): 2792–2800.

13. "Calcium production," can be found under https://mateck.com/en/content/96-calcium-20ca40 (accessed 22 January 2026), (2026).

14. S. Valdez, B. Campillo, and J. J. Islas, "Correlation between Hardness, Structure and Electrochemical Performance of an AlZnMnMg Alloy," *Engineering* 04 (2012): 590–597.

15. A. Shyamsunder, L. E. Blanc, A. Assoud, and L. F. Nazar, "Reversible Calcium Plating and Stripping at Room Temperature Using a Borate Salt," *ACS Energy Letters* 4 (2019): 2271–2276.

16. A. Ponrouch, C. Frontera, F. Bardé, and M. R. Palacín, "Towards a Calcium-Based Rechargeable Battery," *Nature Materials* 15 (2016): 169–172.

17. D. Wang, X. Gao, Y. Chen, L. Jin, C. Kuss, and P. G. Bruce, "Plating and Stripping Calcium in an Organic Electrolyte," *Nature Materials* 17 (2018): 16–20.

18. Q. Li, A. Chen, D. Wang, Z. Pei, and C. Zhi, "Soft Shorts Hidden in Zinc Metal Anode Research," *Joule* 6 (2022): 273–279.

19. O. W. Elkhafif, Y. Zhao, Z. Guo, M. Titirici, T. Jacob, and H. K. Hassan, "Dendrite Formation and Self-Healing Mechanism in Ionic Liquid-Based Magnesium Batteries," *Advanced Energy Materials*. (2026), https://doi.org/10.1002/aenm.202505315.

20. I. Ul Mohsin, S. Riedel, Y. Xiu, Z. Zhao-Karger, and C. Ziebert, "New Insights into Self-Discharge and Heat Generation in Magnesium Batteries," *Batteries & Supercaps* 6 (2023), https://doi.org/10.1002/batt.202300251.

21. Z. Zhao-Karger, Y. Xiu, Z. Li, A. Reupert, T. Smok, and M. Fichtner, "Calcium-Tin Alloys as Anodes for Rechargeable Non- Aqueous Calcium-Ion Batteries at Room Temperature," *Nature Communications* 13 (2022): 3849.

22. Y. Xiu, Z. Li, V. Bhaghavathi Parambath, *et al.*, "Combining Quinone-Based Cathode with an Efficient Borate Electrolyte for High-Performance Magnesium Batteries," *Batteries & Supercaps* 4 (2021): 1850–1857.

23. T. Yamamoto and H. Etori, "Poly(anthraquinone)s Having a π-Conjugation System along the Main Chain. Synthesis by Organometallic Polycondensation, Redox Behavior, and Optical Properties," *Macromolecules* 28 (1995): 3371–3379.

24. *Polishing tool with diamond head, can be found under* https://www.amazon.de/Casfuy-Krallenschleifer- Geschwindigkeiten-leistungsstark-professionell/dp/B08QHHXHS7?th=1(accessed, 5 September 2025), 2025.

Supporting Information

Additional supporting information can be found online in the Supporting Information section.